Journal of Applied Mechanics and Technical Physics, Vol. 47, No. 6, pp. 812–820, 2006

STRUCTURE OF SUPERSONIC TURBULENT FLOWS IN THE VICINITY OF INCLINED BACKWARD-FACING STEPS

I. A. Bedarev and N. N. Fedorova

UDC 532.517.2 : 532533.601.155

Supersonic ($M_\infty = 2$–5) turbulent flows in the vicinity of a two-dimensional backward-facing step with an inclined leeward side are considered by methods of mathematical modeling. The wave structure of the flow with a varied angle of inclination of the leeward side of the step and a varied free-stream Mach number is considered.

Key words: *supersonic flows, shock waves, boundary layer, turbulence.*

Introduction. The problem of a supersonic flow past various steps is a classical problem of aerodynamics. Steps with different angles of inclination of the leeward side are frequent elements of the surface of flying vehicles and their propulsion units. Such a configuration is used to organize and stabilize combustion in air-breathing engines. In addition, the problem of the flow past a step is intimately related to the problem of the flow in the base region and in the near wake behind a flying vehicle entering the atmosphere. A detailed review of research performed in this field in 1950s–1970s can be found in [1, 2]. The first analytical study of the flow past a 90° backward-facing step (BFS) was performed in [3] under the assumption that there exists a streamline dividing the separation region and the external part of the flow. An alternative method of integral moments, which was proposed in [4] and which was first used to describe the flow in the vicinity of a step in [5], is based on the hypothesis that there exists a "free jet" emanating from the rib of the body and a stagnant base region providing compression necessary for flow deflection.

In earlier experimental works [6, 7], the main attention was paid to measuring the static pressure in the base region, because it exerts a significant effect on the drag of the body. The wave structure of the flow was studied in later papers [8–10]. Much attention is currently paid to large-scale vortex structures developing in the mixing layer above the separation region and playing an important role in mass, momentum, and energy transfer between the recirculation zone and the external inviscid flow [11].

The base flow is studied by methods of mathematical modeling incorporating simplified models [12] and full Navier–Stokes equations [13–16].

In the present work, we consider the flow in the vicinity of a two-dimensional BFS with an inclined leeward side. The study is performed for moderate angles of inclination of the faces, which is of interest for analyzing the boattailing effect. It is known that a change in the shape of the base part of the body [preliminary expansion with a small (up to 15°) angle] leads to an increase in pressure in the base region and, hence, to a decrease in drag of the body [17, 18].

Some configurations computed in the present work were examined experimentally in [19]; in turn, the experimental results of [19] were used for verification of computations. In [20, 21], the same flows were studied numerically with the use of the full averaged Navier–Stokes equations supplemented by various semi-empirical models of turbulence. We also computed similar configurations previously [22]. Because of restrictions caused by a small size of the computational domain and an insufficiently refined grid, however, the detailed structure of the flow was not obtained in those computations.

Khristianovich Institute of Theoretical and Applied Mechanics, Siberian Division, Russian Academy of Sciences, Novosibirsk 630090; bedarev@itam.nsc.ru; nfed@itam.nsc.ru. Translated from Prikladnaya Mekhanika i Tekhnicheskaya Fizika, Vol. 47, No. 6, pp. 48–58, November–December, 2006. Original article submitted December 21, 2005; revision submitted January 30, 2006.

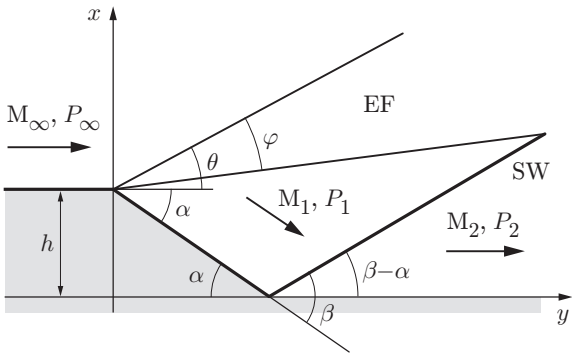

Fig. 1. Wave pattern of an inviscid flow past a step: the expansion fan and shock wave are denoted by EF and SW, respectively.

TABLE 1

Parameters of Inviscid Flows Past Steps

M_∞	α, deg	θ, deg	φ, deg	M_1	P_1/P_∞	β, deg	P_2/P_1	P_2/P_∞	M_2
2	8	30	12	2.3	0.62	32.4	1.6	1.0	1.992
	15		25	2.6	0.39	35.8	2.54	0.996	1.95
	25		39	3.1	0.19	43.4	5.12	0.95	1.76
	45		52	4.49	0.028	—	—	—	—
2.9	8	20.2	10.5	3.34	0.52	23.5	1.90	0.997	2.88
	25		32.5	4.61	0.097	36.7	8.70	0.84	2.43
	45		57	7.45	0.0053	—	—	—	—
3.75	8	15.5	10	4.37	0.44	19.2	2.26	0.99	3.72
	25		31.5	6.4	0.047	33.9	14.73	0.69	2.9
	45		60	12.48	0.0006	—	—	—	—
5.0	8	12	10	6	0.34	16	2.9	0.98	4.9
	25		30	10	0.013	32	32.5	0.43	3.35

Note. The dash means that there is no solution.

Geometry, Test Conditions, and Wave Patterns of the Flow. A supersonic flow with a static pressure P_∞ is incident onto a step of height h with an angle of inclination of the leeward side α. In an inviscid flow (Fig. 1), the first deflection of the flow (by the angle $-\alpha$) occurs isentropically in the centered expansion wave, and the second deflection (by the angle α) occurs in an oblique shock wave in the compression corner. Table 1 contains the parameters obtained from relations of the ideal gas dynamics: angle of inclination of the first characteristic of the Prandtl–Meyer wave θ, angle φ of the expansion fan, Mach number behind the expansion fan M_1, ratio of the static pressure in the base region to the free-stream pressure P_1/P_∞, angle of inclination of the shock wave β, and flow parameters behind the shock wave M_2 and P_2. For $M_\infty = 5$, the angle $\alpha = 45°$ is close to the critical value ($P_1/P_\infty \approx 10^{-6}$). For lower values of the Mach number (M_∞ = 2–4), the pressure ratio is not that low, but the value $\alpha = 45°$ exceeds the limiting angle of flow deflection in the attached oblique shock wave. It follows from Table 1 that the decrease in static pressure in the Prandtl–Meyer wave P_1/P_∞ is compensated by the increase in pressure in the oblique shock wave only for rather low angles of flow deflection and moderate Mach numbers. If the angle of flow deflection is large, the pressure behind the oblique shock wave is significantly lower than the free-stream value. The static pressure is recovered to P_∞ further downstream, in the shock wave–expansion fan interaction region, which results in degeneration of the shock wave into the Mach line.

The wave pattern of the viscous flow past a step is complicated by interaction of shock and expansion waves with the boundary layer. The flow in the expansion fan passing through the boundary layer in the zone of its deflection is no longer isentropic. The boundary layer can be considered as a sequence of contact discontinuities, each of discontinuities being responsible for refraction and reflection of characteristics of the Prandtl–Meyer wave. This interaction leads to decentering of the characteristics of the Prandtl–Meyer wave, a change in the angle of inclination of these characteristics in the external flow, and formation of a lip shock [8, 9] and a tangential discontinuity line

TABLE 2

Free-Stream Conditions

M	Re_1, m^{-1}	P_0, MPa	T_0, K	δ, mm	δ^*, mm	δ^{**}, mm
2.00	$3.0 \cdot 10^7$	0.198	280	4.35	1.08	0.375
2.90	$3.8 \cdot 10^7$	0.418	265	5.08	1.84	0.380
3.75	$5.8 \cdot 10^7$	1.070	270	4.85	2.04	0.290

located below the lip shock [7]. It follows from the experimental results of [10] that the reduced pressure in the base region affects the flow upstream of the step; the constant-pressure lines in the region of flow expansion are not straight, and the angle of flow deflection is smaller than the total angle of deflection of the Prandtl–Meyer flow necessary to reach the same pressure. The shock wave formed in the compression corner transforms to a system of compression waves closed by the oblique shock wave, which is commonly called the tail shock. Interaction of compression waves with the boundary layer in the compression corner may form a separation region with a separated shock and a shock wave at the reattachment point. The separation zone forms a virtual surface exposed to the external supersonic flow. In the case of a massive separation zone beginning at the end face immediately behind the top corner point, the separated shock can absorb the lip shock.

Experimental measurements show (see, e.g., [9]) that the dimensionless pressure P/P_∞ is recovered to unity in real flows upstream of the point of intersection of the tail shock with the last characteristic of the Prandtl–Meyer wave. In some experiments, the pressure behind the reattachment point exceeds the free-stream pressure. In addition, the pressure-recovery process is nonmonotonic: the distribution contains local maximums disappearing if the shape of the model lip is changed [17]. According to [9], the nonuniformity of pressure recovery may be caused by the action of the lip shock, which is extended to the region behind the tail shock. The local minimums in the measured pressure distributions were attributed in [19, 20] to the action of secondary expansion waves incident onto the model surface from the triple point of the λ-configuration of shock waves formed above the separation region.

In the present work, we consider flows past backward-facing steps with moderate angles of inclination of the leeward side ($\alpha \leqslant 45^\circ$), where the separation region does not occupy the entire inclined face and, hence, the processes that occur in the vicinity of the expansion corner and in the separation region are divided in space. The step geometry is shown in Fig. 1. The computations were performed for $h = 15$ mm and $\alpha = 8$–45°. The free-stream parameters of the examined flows (total pressure P_0, total temperature T_0, and dimensional Reynolds number Re_1) and the integral characteristics of the boundary layer upstream of the interaction region (thickness δ, displacement thickness δ^*, and momentum thickness δ^{**}) are listed in Table 2. These parameters describe the real test conditions of the T-313 wind tunnel based at the Khristianovich Institute of Theoretical and Applied Mechanics of the Siberian Division of the Russian Academy of Sciences where the tests were performed [19].

Mathematical Model, Boundary Conditions, and Computation Method. The computations were performed with the use of the Favre-averaged Navier–Stokes equations supplemented by Wilcox's k–ω model of turbulence. A four-step scheme of splitting in terms of physical processes and spatial variables was used for approximation in time. The spatial derivatives of inviscid fluxes were approximated by a third-order total variation diminishing (TVD) scheme constructed on the basis of splitting of the flux vector in terms of physical processes; viscous terms were approximated by central differences with second-order accuracy. The majority of computations were performed on a regular grid refined toward the surface. Depending on the computational-domain size, the grid contained 400–600 nodes in the x direction and 200–300 nodes in the y direction (80–100 nodes were located in the boundary-layer region). The minimum step in the normal-to-wall direction was approximately $10^{-4}h$. The convergence was checked by computations on consecutively refined grids (200×150, 300×200, and 400×300 nodes), which revealed that the solution remained unchanged beginning from the grid that contained 300×200 nodes.

The input conditions for the computational domain were the profiles of all mean and turbulent parameters, which were obtained by numerically solving the problem on a flat plate and whose integral parameters were close to experimental ones. A detailed description of the model, algorithm, and boundary conditions can be found in [23].

Computation Results. Figure 2 shows the distribution of the dimensionless pressure along the surface for $\alpha = 8^\circ$ and different values of M_∞. The flow is attached for all Mach numbers. The solutions obtained are consistent with the experimental data of [19]. A comparison of the computed results with the inviscid solution shows that the effect of reduced pressure upstream from the expansion corner in all cases is significant at a distance of the order

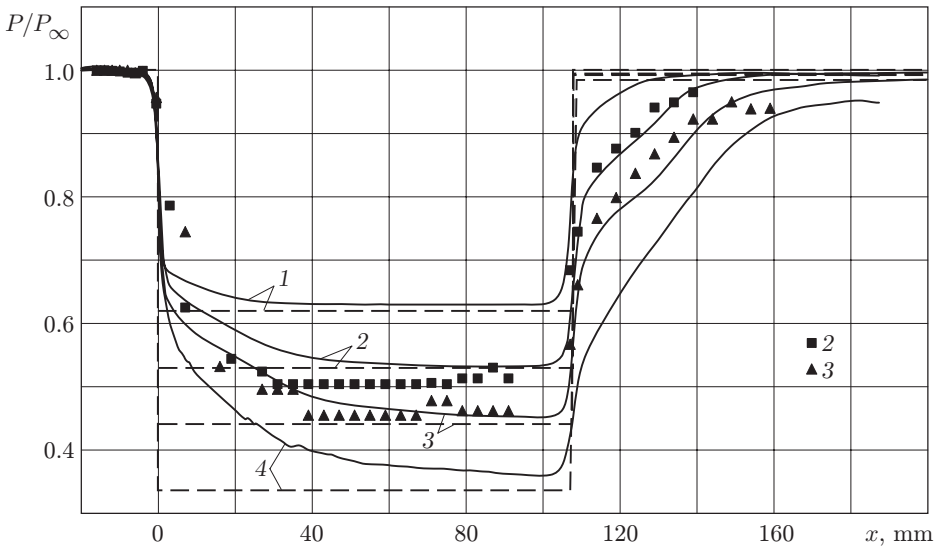

Fig. 2. Pressure distribution along the surface for $\alpha = 8^\circ$ and $M_\infty = 2$ (1), 2.9 (2), 3.75 (3), and 5 (4): the solid curves show the computation results, the dashed curves describe the inviscid solution, and the points are the experimental results of [19].

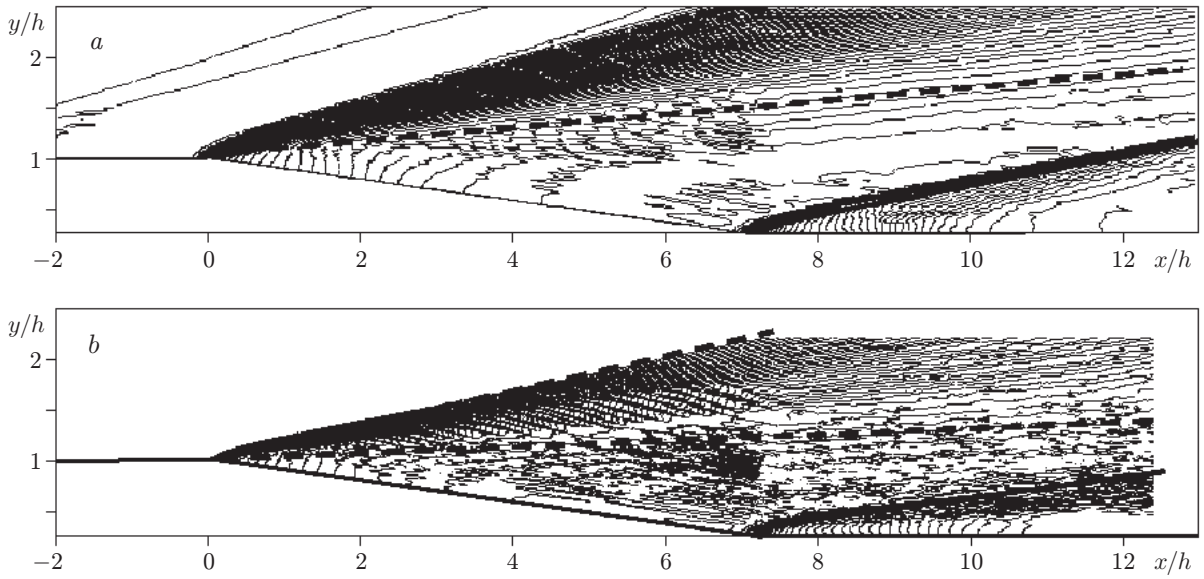

Fig. 3. Static pressure isolines for $\alpha = 8^\circ$ and $M_\infty = 3.75$ (a) and 5 (b); the dashed curves show the limiting characteristics of the Prandtl–Meyer wave.

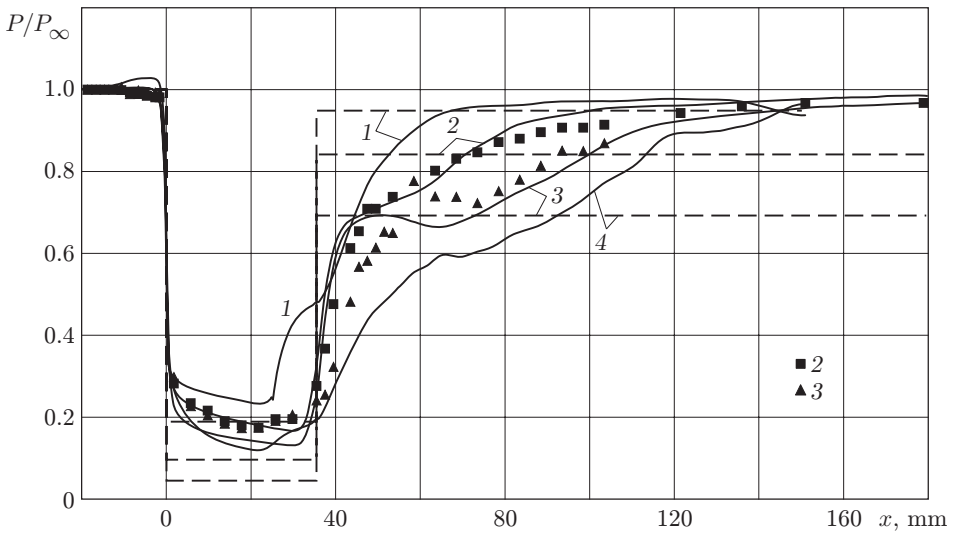

Fig. 4. Pressure distribution along the surface for $\alpha = 25°$ (notation the same as in Fig. 2).

of the boundary-layer thickness. The pressure on the inclined face gradually decreases to a value corresponding to the inviscid flow, and the pressure behind the compression corner is recovered to P_∞. As the Mach number increases, however, the viscous solution in zones of interaction of the boundary layer with the expansion and shock waves becomes more and more different from the inviscid solution. Figure 3 shows the isolines of static pressure for $\alpha = 8°$ and $M_\infty = 3.75$ and 5.00. The dashed curves show the limiting characteristics of the inviscid Prandtl–Meyer wave. The presence of a viscous boundary layer leads to decentering of the expansion fan; therefore, the extreme right characteristics impinge on the fan and interact with the latter, which leads to formation of reflected waves incident onto the inclined face. A rather complicated interaction gives rise to secondary waves affecting the flow downstream. In particular, the action of these waves decelerates the decrease in pressure behind the expansion fan and leads to a slower increase in pressure behind the oblique shock.

As the angle of inclination of the BFS leeward side increases to $\alpha = 25°$, the flow structure becomes different (Fig. 4). It should be noted that the base pressure is higher than that in an inviscid flow for all Mach numbers, which may be caused by an insufficient length of the inclined face. A separation is observed in the vicinity of the compression corner for all Mach numbers considered, which is supported by the presence of a typical plateau in the pressure distribution. Further downstream of the reattachment point, the pressure-distribution curves have an inflection, and the pressure in this region is close to the pressure behind the oblique shock predicted by the inviscid model. An analysis of the computed isolines of static pressure, Mach numbers, and local angles of flow deflection for $M_\infty = 3.75$ and $\alpha = 25°$ (Fig. 5) offers an explanation of the change in pressure behind the reattachment point. The angle of inclination of the first characteristic of the expansion wave coincides with the value predicted by the inviscid theory, viscous effects being responsible for wave decentering. The limiting (right) characteristics of the expansion wave are immersed into the viscous layer; therefore, the maximum value of the Mach number in the real flow is lower than the value predicted by the inviscid theory. Nonuniformity of pressure isolines and distortion of their shape, which is fairly significant in the expansion-fan portion that passed through the region of the drastic deflection of the viscous layer, are also worth noting. A monotonic increase in pressure is first observed behind the compression corner; the pressure isolines are inclined toward the tail shock. After that the slope of isolines changes: characteristics of another family of compression waves arrive on the surface, are reflected from the surface, and catch up with the main shock. Compression waves of another family arise as the shock wave passes through a denser mixing layer. The reason for their formation is, possibly, reflection of the shock wave leaving the base region with a reduced density from the mixing layer with a higher density. The presence of compression waves of different families is responsible for the nonuniform growth of pressure on the surface (see Fig. 4).

Thus, the reason for formation of a new system of compression waves is interaction of the oblique shock with the mixing layer detached from the BFS surface; the upper and lower boundaries of the mixing layer are seen in the

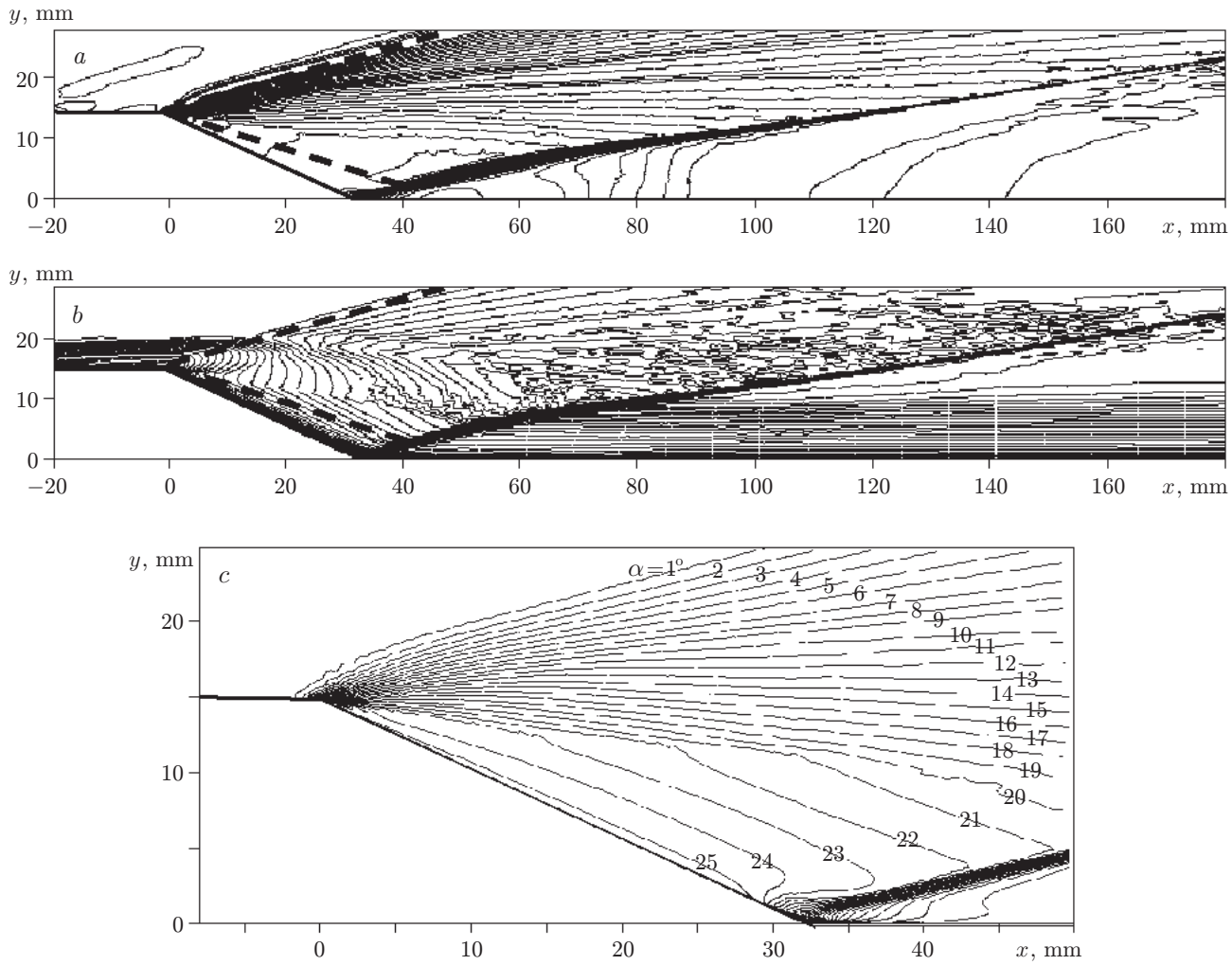

Fig. 5. Computed isolines of static pressure (a), Mach numbers (b), and local angles of flow deflection (c) for $M_\infty = 3.75$ and $\alpha = 25°$: the dashed curves are the limiting characteristics of the Prandtl–Meyer wave.

pattern of Mach number isolines (see Fig. 5). A comparison of data in Figs. 5a and 5b shows that the wave system responsible for the increase in pressure behind the tail shock arises in the region where the tail shock passes through the mixing layer, which is also evidenced by the change in the angle of shock-wave inclination. An analysis of local flow deflections shows that the flow in the region where the secondary compression waves (reflected from the mixing layer) arrive is directed toward the surface. This supports the conclusion that the increase in pressure on the surface is caused by the presence of a denser mixing layer, which does not turn to a necessary angle when passing through the shock wave. Flow alignment in the direction parallel to the wall occurs in additional compression waves, which induce an increase in pressure on the wall to P_∞. The intensity of reflected waves is determined by the properties of the separated mixing layer, and their position depends on the BFS height and on the thickness of the boundary layer flowing down.

Figure 5c shows the isolines of the velocity-vector direction (local deflections of the flow). The maximum angle $\alpha = 25°$ is observed only for gas particles located near the step surface, whereas the main part of the flow turns by an angle $\alpha < 20°$. Figure 5c shows a line beginning on the BFS face, and the slope of the velocity vector changes along this line. A comparison of Figs. 5b and 5c allows us to assume that there exists a contact discontinuity line (lower boundary of the mixing layer) or a jet shed from the model lip. A similar "slip line" was observed in the experiment [7]. Apparently, flow stratification occurs in the vicinity of the external corner of the model: the viscous near-wall low-velocity region turns by a "necessary" angle and forms the base region with low density and

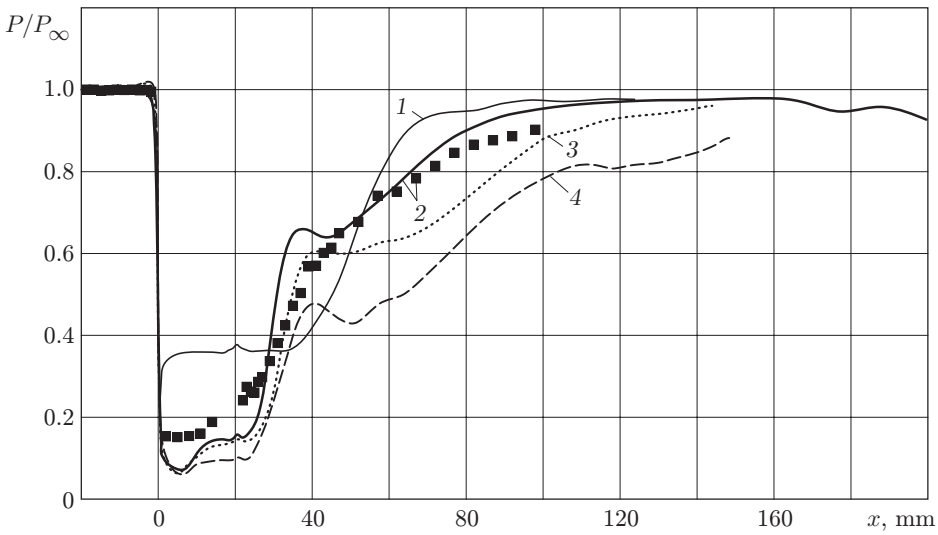

Fig. 6. Pressure distribution along the surface for $\alpha = 45^\circ$ and $M_\infty = 2$ (1), 2.9 (2), 3.75 (3), and 5 (4): the curves refer to the computed data and the points refer to the experimental results of [19].

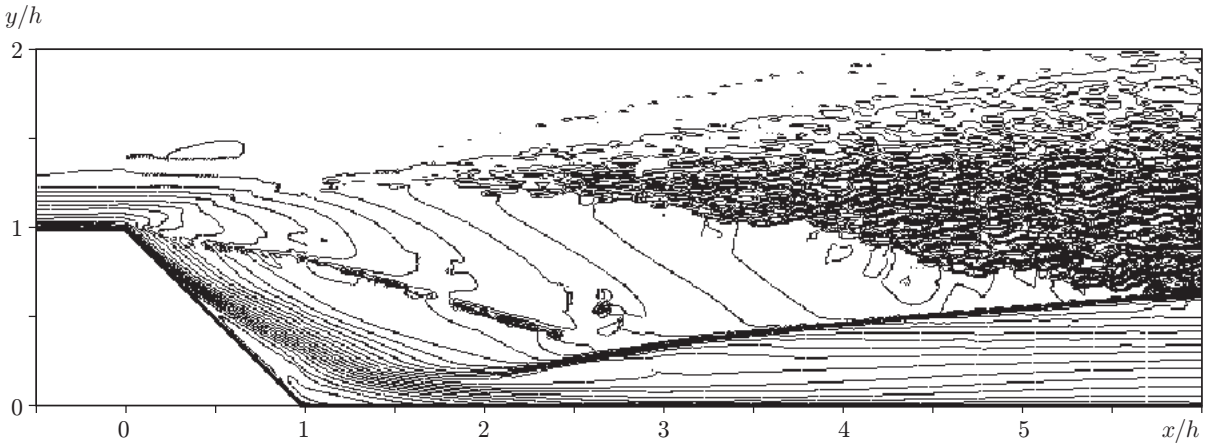

Fig. 7. Mach number isolines near the step for $\alpha = 45^\circ$ and $M_\infty = 5$.

pressure, whereas the external high-velocity flow moves away from the surface and forms a mixing layer with a higher density. "Stratification" enhances with increasing free-stream Mach number. This process is expected to be significantly affected by the free-stream Reynolds number and integral boundary-layer thicknesses determining the distribution of gas-dynamic parameters in the boundary layer.

Figure 6 shows the computed pressure distribution along the surface for the maximum examined angle $\alpha = 45^\circ$. The behavior of the curves is similar to the behavior of the curves in Fig. 4 for $\alpha = 25^\circ$; in the case with $\alpha = 45^\circ$, however, the separation region is more extended. For $M_\infty = 2$, the pressure plateau begins immediately behind the external corner. For high values of the Mach number, the separation region is smaller, and its length remains unchanged. Pressure recovery behind the reattachment point occurs nonuniformly. For $M_\infty > 2$, the tail shock is followed by a local maximum with a subsequent small decrease in pressure, which is caused by arrival of secondary expansion waves emanating from the triple point of the λ-configuration of shock waves formed above the separation region. Then the pressure increases again; at high Mach numbers, the pressure is recovered to the free-stream value slower than at low Mach numbers.

Figure 7 shows the Mach number isolines for $M_\infty = 5$. One can see the "jet" shed from the model lip with clearly expressed upper and lower boundaries. The data presented in Fig. 7 also support the conclusions of the experimental research [10] that the flow in the vicinity of the expansion corner is not isentropic. The flow is vortical

in the region of curved pressure isolines. The vortices propagating downstream reach the tail shock and pass through the latter, inducing pressure fluctuations on the model surface rather far downstream from the interaction region. If the level of free-stream turbulence is low, the vortex intensity increases, and they exert a significant effect on the distribution of pressure and other characteristics of the flow. There are no pressure oscillations if the turbulence level exceeds 2%.

Conclusions. Based on numerical research of supersonic flows in the vicinity of backward-facing steps at $M_\infty = 2$–5, wave patterns of the flow are constructed for different step angles and Mach numbers. It is shown that the presence of a viscous boundary layer alters the flow properties in the vicinity of the expansion corner. In particular, decentering and curving of constant-pressure lines of the expansion fan are observed. For small angles of the step face, the flow does not separate from the surface, but the secondary waves induced by decentering of the expansion wave and its interaction with the boundary layer slow down the pressure recovery to the level determined by the inviscid theory. This effect becomes more pronounced with increasing free-stream Mach number.

As α increases, there appears a local separation region in the compression corner; the length of this region increases with increasing α. The flow past the expansion corner leads to stratification of the viscous flow. The viscous near-wall low-velocity low-density flow turns by the angle α, and a rarefied base region is formed. The external high-velocity and denser region of the boundary layer turns by an angle smaller than α in passing through the expansion wave and forms a mixing layer moving away from the wall.

Reconstruction of pressure behind the compression corner occurs in the oblique shock and in additional compression waves formed in the zone of interaction of the tail shock with the mixing layer. The existence of a system of secondary waves consecutively reflected from the model surface and the main shock wave can lead to formation of local extreme points in the static pressure distribution and also affect the distributions of friction and heat fluxes along the surface.

This work was supported by the Russian Foundation for Basic Research (Grant No. 05-01-00684).

REFERENCES

1. L. V. Gogish and G. Yu. Stepanov, *Turbulent Separated Flows* [in Russian], Nauka, Moscow (1979).
2. A. P. Shvets and I. T. Shvets, *Near-Wake Gas Dynamics* [in Russian], Naukova Dumka, Kiev (1976).
3. D. R. Chapman, "An analysis of the base pressure at supersonic velocities and comparison with experiment," Tech. Report NACA, No. 1051 (1951).
4. L. Crocco and L. Lees, "A mixing theory for the interaction between dissipative flows and nearly isentropic streams," *J. Aeronaut. Sci.*, **19**, No. 10, 649–679 (1952).
5. J. Rom, "Analysis of the near wake pressure in supersonic flow using the momentum integral method," *J. Spacecraft Rockets*, **3**, No. 10, 1504–1509 (1966).
6. S. M. Bogdonoff, "A preliminary study of Reynolds number effects on base pressure at M = 2.95," *J. Aeronaut. Sci.*, **19**, No. 3, 201–206 (1952).
7. A. F. Charwat and J. K. Yakura, "An investigation of two-dimensional supersonic base pressure," *J. Aeronaut. Sci.*, **25**, No. 2, 122–128 (1958).
8. S. Weinbaum, "Rapid expansion of a supersonic boundary layer and its application to the near wake," *AIAA J.*, **4**, 217–226 (1966).
9. F. R. Hama, "Experimental studies on the lip-shock," *AIAA J.*, **23**, No. 2 (1968).
10. M. G. Scherberg and H. E. Smith, "An experimental study of supersonic flow over a rearward facing step," *AIAA J.*, **5**, No. 1, 51–56 (1967).
11. K. M. Smith and J. C. Dutton, "Investigation of large-scale structures in supersonic planer base flows," *AIAA J.*, **34**, No. 6, 1146–1152 (1996).
12. W. L. Hankey and E. J. Cross (Jr.), "Approximate closed-form solutions for supersonic laminar separated flows," *AIAA J.*, **5**, No. 4, 651–654 (1967).
13. V. M. Kovenya and A. S. Lebedev, "Numerical simulation of laminar and turbulent wake flows," *Vychisl. Tekhnol.*, **2**, No. 6, 42–52 (1997).
14. J. Sahu, "Numerical computations of supersonic base flow with special emphasis on turbulence modeling," *AIAA J.*, **32**, No. 7, 1547–1549 (1994).

15. C. C. Chuang and C. C. Cheing, "Supersonic base-flow computation using high-order closure turbulence models," *J. Spacecraft Rockets*, **33**, No. 3, 374–380 (1996).
16. Yu. Halupovich, B. Natan, and J. Rom, "Numerical solution of the turbulent supersonic flow over backward facing step," *Fluid Dynam. Res.*, **24**, No. 2, 251–273 (1999).
17. A. Roshko and C. L. Thomke, "Effect of a shoulder modification on turbulent supersonic base flow," *AIAA J.*, **5**, No. 4, 827–829 (1966).
18. C. J. Bourdon and J. C. Dutton, "Effect of boattailing on the turbulence structure of a compressible base flow," *J. Spacecraft Rockets*, **38**, No. 4, 534–541 (2001).
19. A. A. Zheltovodov, V. M. Trofimov, E. Kh. Shülein, and V. N. Yakovlev, "Documented data of experimental studies of supersonic turbulent separated flows near inclined steps," Report No. 2030, Inst. Theor. Appl. Mech., Sib. Div., Acad. of Sci. of the USSR, Novosibirsk (1990).
20. A. A. Zheltovodov, E. Kh. Shülein, and C. C. Horstman, "Development of separation in the region where a shock interacts with a turbulent boundary layer perturbed by rarefaction waves," *J. Appl. Mech. Tech. Phys.*, **34**, No. 3, 346–353 (1993).
21. A. V. Borisov and V. B. Karamyshev, "Method of the numerical study of turbulent separated flows," Preprint No. 9-88, Inst. Theor. Appl. Mech., Sib. Div., Acad. of Sci. of the USSR, Novosibirsk (1988).
22. I. A. Bedarev and N. N. Fedorova, "Computation of gas-dynamic parameters and heat transfer in supersonic turbulent separated flows near backward-facing steps," *J. Appl. Mech. Tech. Phys.*, **42**, No. 1, 49–56 (2001).
23. A. V. Borisov and N. N. Fedorova, "Computation of turbulent separated flows by a method with an increased order of approximation," *Teplofiz. Aéromekh.*, **2**, No. 3, 253–269 (1995).